Chemical Science

www.rsc.org/chemicalscience

Volume 3 | Number 12 | December 2012 | Pages 3333–3544

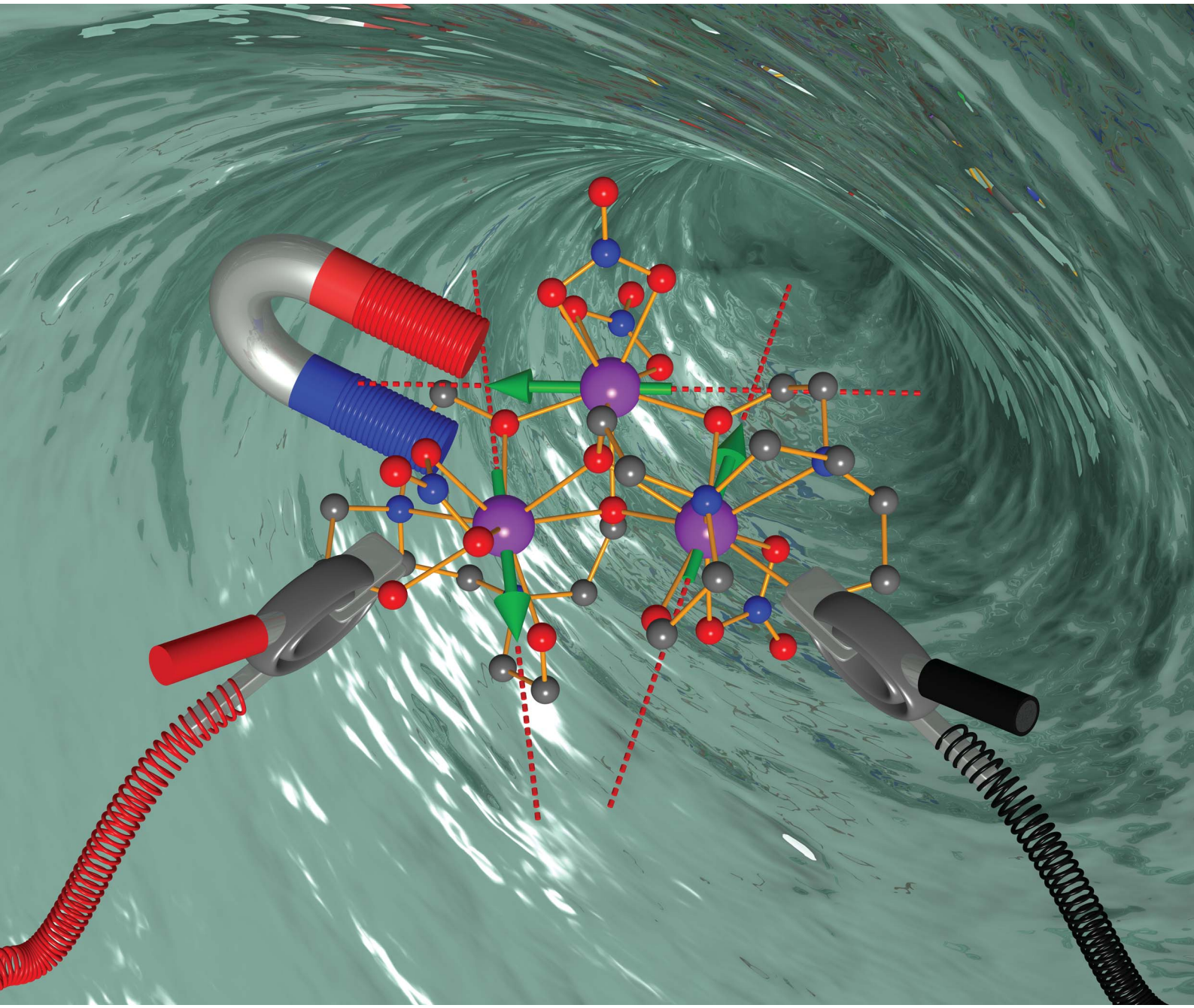

ISSN 2041-6520

RSC Publishing

EDGE ARTICLE

Wei Shi, Yanhua Lan, Liviu F. Chibotaru, Peng Cheng *et al.*

A single-molecule magnet assembly exhibiting a dielectric transition at 470 K

2041-6520(2012)3:12;1-O

Chemical Science

Dynamic Article Links

Cite this: *Chem. Sci.*, 2012, **3**, 3366

www.rsc.org/chemicalscience

EDGE ARTICLE

A single-molecule magnet assembly exhibiting a dielectric transition at 470 K†

Yu-Xia Wang,[a] Wei Shi,*[a] Han Li,[a] You Song,[b] Liang Fang,[c] Yanhua Lan,*[d] Annie K. Powell,[d] Wolfgang Wernsdorfer,[e] Liviu Ungur,[f] Liviu F. Chibotaru,*[f] Mingrong Shen[c] and Peng Cheng*[a]

Received 20th July 2012, Accepted 24th September 2012
DOI: 10.1039/c2sc21023a

A triangular Dy(III) single-molecule magnet (SMM) exhibiting ferroelectric bistability is assembled in an acentric space group $Pna2_1$. Hysteresis loops associated with its SMM behavior together with a two-step slow relaxation of the magnetization are observed below 30 K. A transition with dielectric anomalies between a paraelectric and a ferroelectric phase occurs at 470 K.

Molecules or molecular assemblies with various functionalities are currently of great interest in coordination chemistry due to their great potential for application as new types of high-density memory devices.[1] One of the attractive multifunctional materials are multiferroics, in which both magnetic and ferroelectric bistabilities coexist within a single material.[2] However, single-phase multiferroics are rare because the mechanisms that drive ferroelectricity and ferromagnetism are mutually exclusive.[3] Hitherto the majority of well-studied multiferroics are atom-based materials such as particular perovskite oxides.[4] Only very recently a few molecule-based porous crystalline metal-organic frameworks (MOFs) have been reported to display both magnetic and ferroelectric properties, representing a new class of multiferroic materials.[5]

To further miniaturize the molecular devices, using one or a few magnetic molecules such as single-molecule magnets (SMMs) to generate materials which also show ferroelectric properties should be particularly attractive. In such a case, the systems will combine the advantages of the molecular scale with the properties of bulk magnetic materials into one single material. As known, a material assembled in a polar point space group is likely to become a highly polarizable system, which is one of the basic requirements for showing ferroelectricity.[5c,d] Along this line, molecular ferroelectrics could consequently be realized if SMMs were assembled in a polar space group by a chemical method. However, no examples have been explored.

In recent years, of the lanthanide ions, Dy(III) has become a good source of ions to generate thousands of SMMs. Some of them represent considerably high energy barriers.[6] Herein we report an interesting new trinuclear Dy(III) SMM, namely $[Dy_3(HL)(H_2L)(NO_3)_4]$ ethanol (**Dy_3L**, H_4L = *N*,*N*,*N*′,*N*′-tetrakis(2-hydroxyethyl)-ethylene-diamine), crystallized in an acentric space group $Pna2_1$, belonging to one of the ten polar point groups.‡ **Dy_3L** exhibits not only SMM behaviour with a two-step slow relaxation of the magnetization at low temperatures with characteristic hysteresis loops, but also dielectric hysteresis loops and a phase transition with the dielectric anomalies at 470 K.

Single-crystal structural data of **Dy_3L** at different temperatures varying from 120 to 463 K were determined, showing that **Dy_3L** crystallizes in the orthorhombic space group $Pna2_1$ (Table S1†). The structure at room temperature is depicted in Fig. 1a. Dy2 is in a distorted square antiprismatic coordination sphere, satisfied with four oxygens from the ligands and four oxygens from nitrates; however, the coordination geometries of Dy1 and Dy3 are distorted capped square antiprisms, completed by five oxygens and two nitrogens from the ligands and two oxygens from nitrate. Pairs of Dy(III) ions except for Dy1···Dy3 are mono-bridged by a μ_2-O from the ligand; and the three Dy(III) ions are further doubly bridged by two μ_3-O from ligands forming a pseudo-isosceles triangle, surrounded by two ligands and four nitrates. The Dy···Dy distances within the triangle are 3.488(1), 3.509(1) and 3.898(1) Å, respectively. As shown in Fig. 1b and S1a,† each asymmetric unit contains four **Dy_3L** molecules which reside in different positions in the cell. There are weak hydrogen bonding interactions ($O5–H5\cdots O11_{NO_3^-}$) between neighboring **Dy_3L** units with an O···O distance of 2.918 Å. And the **Dy_3L** unit is further connected to an ethanol

[a]*Department of Chemistry and Key Laboratory of Advanced Energy Materials Chemistry (MOE), Nankai University, Tianjin 300071, P. R. China. E-mail: shiwei@nankai.edu.cn; pcheng@nankai.edu.cn*
[b]*State Key Laboratory of Coordination Chemistry, Nanjing National Laboratory of Microstructures, School of Chemistry and Chemical Engineering, Nanjing University, Nanjing 210093, P. R. China*
[c]*Department of Physics and Jiangsu Key Laboratory of Thin Films, Soochow University, Suzhou 215006, P. R. China*
[d]*Institute of Inorganic Chemistry, Karlsruhe Institute of Technology, Engesserstrasse 15, 76131 Karlsruhe, Germany. E-mail: yanhua.lan@kit.edu*
[e]*Institut Néel—CNRS, BP 166, 25 Avenue des Martyrs, 38042 Grenoble Cedex 9, France*
[f]*Division of Quantum and Physical Chemistry, Katholieke Universiteit Leuven, Celestijnenlaan 200F, B-3001, Heverlee, Belgium. E-mail: Liviu.Chibotaru@chem.kuleuven.be*

† Electronic supplementary information (ESI) available: Materials and methods, crystallographic study, computational details of the *ab initio* calculations and crystallographic data (CIF). CCDC reference number 853328. For ESI and crystallographic data in CIF or other electronic format see DOI: 10.1039/c2sc21023a

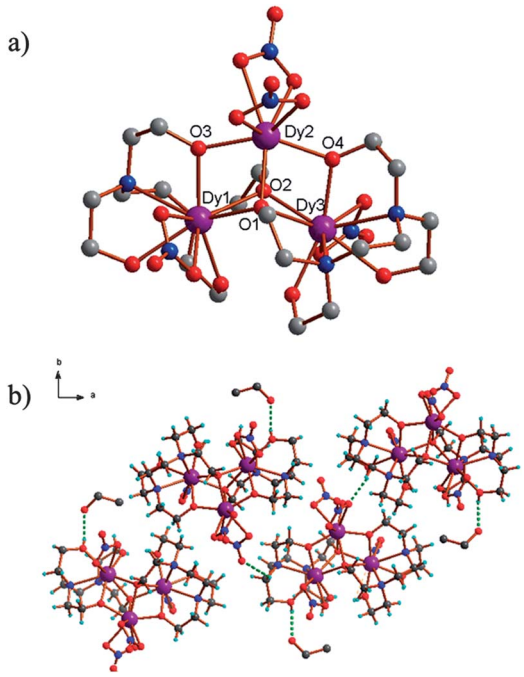

Fig. 1 (a) The trinuclear unit of **Dy_3L**. Hydrogen atoms are omitting for clarity. Color scheme: purple Dy, red O, grey C, blue N. (b) Each unit cell contains four **Dy_3L** molecules connected by hydrogen bonds indicated as green dashed lines.

molecule by another H-bond O8–H8···O21$B_{ethanol}$ with an O···O distance of 2.660 Å (Fig. 1b). As a result, a three-dimensional supramolecular network is constructed by the **Dy_3L** units linked through hydrogen bonding interactions. It is also worth pointing out that the trinuclear **Dy_3L** units and the disordered ethanol molecules surround the 2_1 screw axis, which is also the *c* axis of the crystal (Fig. S1b†).

The static magnetic properties of **Dy_3L** were investigated on a powdered average polycrystalline sample in the temperature range of 2–300 K at 0.1 T. The room-temperature χT value of 40.83 cm^3 K mol^{-1} is in good agreement with that expected 42.51 cm^3 K mol^{-1} for three uncoupled Dy(III) ions ($J = 15/2$, $g = 4/3$, $L = 5$).[7] The χT decreases gradually until ~20 K and then drops abruptly to a minimum of 6.83 cm^3 K mol^{-1} at 2 K (Fig. 2), indicating the progressive depopulation of the excited Stark sublevels of Dy(III) ions and/or weak intra/inter-molecular magnetic interactions. *Ab initio* calculations were carried out to study the nature of the magnetic interactions. Details of the calculation were given in the ESI and are illustrated as Fig. S2–S5 and Tables S2–S5.† The magnetic interactions within **Dy_3L** units include dipolar interactions J_{ij}^{dip} and exchange interactions J_{ij}^{exch}. The total interaction between Dy sites is then described by $J_{ij} = J_{ij}^{dip} + J_{ij}^{exch}$. The dipolar interactions are calculated using the *ab initio* results for the *g* tensor in the ground state of three Dy fragments (Table 1). Two independent exchange parameters were employed in **Dy_3L**: one for coupling of Dy2–Dy1/Dy3 and the other for Dy1–Dy3. These exchange parameters were derived from the simultaneous fit of χT and $M(H)$ curves (Fig. 2 and S2†). The obtained parameters (Table 2) describe the non-collinear Ising exchange interaction between the lowest Kramers doublets on Dy sites in **Dy_3L**:

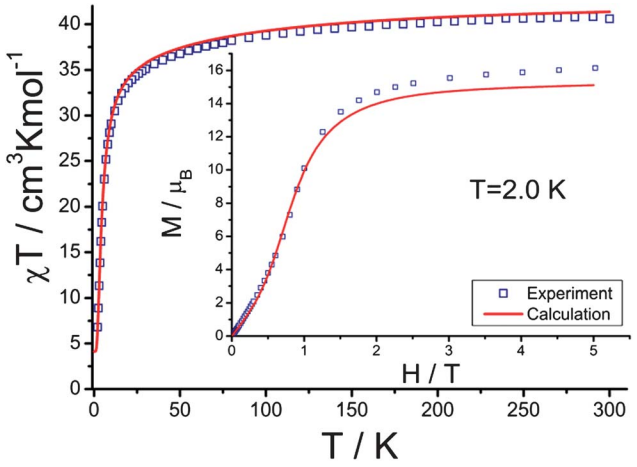

Fig. 2 Temperature dependence of the χT product for **Dy_3L**. The red line is the *ab initio* calculated curve. Inset: molar magnetization at 2 K.

$$H = -J_{12}\hat{S}_{1z}\hat{S}_{2z} - J_{13}\hat{S}_{1z}\hat{S}_{3z} - J_{23}\hat{S}_{2z}\hat{S}_{3z} \quad (1)$$

where $\hat{S}_{iz}$ is the projection of the effective spin 1/2 on the local anisotropy axis *z* of the site i (Fig. 3). The signs of the J_{ij} parameters in Table 2 depend of course on the choice of the positive direction at each local axis *z*. The convention used here is that the latter coincide with the directions of the corresponding green arrows in Fig. 3.

The obtained parameters J_{ij} favor the toroidal alignment of local magnetic moments of **Dy_3L** (Fig. 3). In fact, the dipolar magnetic interaction alone (*i.e.*, setting $J^{exch} = 0$ in the expressions for *J* in Table 2) already favors the toroidal arrangement of the local magnetic moments. Although the exchange interaction parameters are weaker, they have the same signs as the dipolar ones (Table 2) and, therefore, corroborate to further stabilization of the circular arrangement of local magnetic moments (Fig. 3). The spectrum of low-lying exchange Kramers doublets and their *g* tensors are given in Table S4.† The high-field magnetization data represented as the *M vs. H*/*T* curves exhibit non-superposition and indicate the presence of a significant magnetic anisotropy (Fig. S6†). The maximum magnetization at 2 K and 5 *T* is 16.1 μ_B, in agreement with the expected value of 15.7 μ_B for three free Dy(III) ions (Fig. 2, inset). The linear slope above 2 *T*

Table 1 Energies and *g* tensors of the lowest spin–orbit states (cm^{-1})

KD	Dy1	Dy2	Dy3
1	0.000	0.000	0.000
2	108.778	239.577	225.784
3	202.571	459.170	485.721
4	286.735	546.174	634.670
5	322.050	587.706	672.382
6	385.913	642.290	711.704
7	458.087	709.691	753.551
8	524.465	979.880	834.336
Main values of the g-tensor for the lowest doublets			
g_X	0.0528	0.0020	0.0024
g_Y	0.0793	0.0024	0.0028
g_Z	19.7092	19.8247	19.8525
Angle between the main magnetic axis g_Z and the Dy3 plane (degrees)			
	6.657	0.568	10.398

Table 2 The parameters of the dipolar and exchange magnetic interactions (in cm^{-1})

Interaction between centers	J_{ij}^{exch}	J_{ij}^{dip}	$J_{ij} = J_{ij}^{dip} + J_{ij}^{exch}$
1–2	1.608	5.428	7.036
2–3	1.608	5.293	6.901
3–1	1.311	2.959	4.270

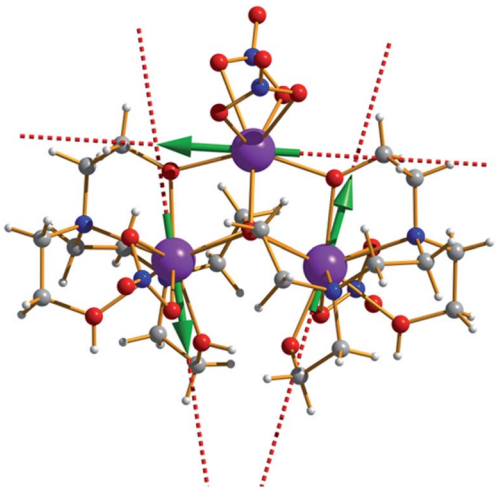

Fig. 3 Calculated local anisotropy axes on Dy(III) sites (dashed lines) and the local magnetic moments in the ground state (arrows).

reflects the admixture of the excited Stark levels on Dy(III) sites by the Zeeman interaction. Both low-temperature χT and low-field $M(H)$ show non-negligible positive slopes, which points to a nonvanishing magnetic moment in the Kramers doublet of **Dy_3L**. This situation differs from the previously investigated Dy_3 triangle,[8] where the ground state was found non-magnetic, explained by a relative 120° arrangement of anisotropy axes on Dy(III) ions.[9] However, in **Dy_3L** this is not the case anymore, because the three Dy(III) ions form an isosceles rather than an equilateral triangle (Fig. 1). The relative orientations of the main anisotropy axes lie almost in the plane of the **Dy_3L** triangles (dashed lines in Fig. 3) and the angles between the main anisotropy are listed in Table 3. As a result the local magnetic moments in the ground Kramers doublet (arrows in Fig. 3) do no compensate each other anymore, which is the reason why **Dy_3L** remains magnetic till very low temperatures.

Alternating current (ac) susceptibility measurements were carried out for **Dy_3L** as functions of both temperature and frequency under a zero-static field to study the dynamics of the magnetization. Both the temperature- and frequency-dependent out-of-phase ac signals (χ'') exhibit two distinct peaks (Fig. S7 and S8†), indicating the possibility of multiple relaxation processes. As already discussed in the structural part and the calculations, **Dy_3L** comprises two types of Dy(III) ions with different coordination spheres forming a weakly coupled molecular system. Therefore, the two χ'' peaks may result from the spin noncolinearity of these two types of Dy(III) ions within each molecule, probably as well as in the crystal packing of molecules. This similar scenario is actually not uncommonly observed in several Dy(III)-based systems.[6b,c,10] To understand the nature of the relaxation processes, two sets of the temperature-dependent χ'' data in relation with two relaxation regimes (a fast relaxation process from 3 to 9 K and a slow relaxation process from 6 to 22 K) were analysed by the Arrhenius law (Fig. S9†), giving the effective energy barriers (Δ) of 42.6 K and 90.9 K with pre-exponential factors (τ_0) of 1.0×10^{-6} s and 5.8×10^{-7} s, respectively. Furthermore, fitting of the Cole–Cole plots by the generalized Debye functions gives α_1 values of 0.26–0.49 and α_2 values of 0.41–0.57, respectively (Fig. S10 and Table S6†). The relatively large α values suggest the moderate distribution of the relaxation time for each process, further indicating the presence of multiple relaxation processes in **Dy_3L**.[6b,c,10,11]

A single crystal of **Dy_3L** was further studied using the micro-SQUID technique to confirm its SMM behavior (Fig. 4).[12] The coercivities of the hysteresis loops increase upon decreasing

Table 3 Angles between the main anisotropy axes on Dy sites

Angles between the main anisotropy axes (degrees)			
	Dy1	Dy2	Dy3
Dy1	0	77.97	25.10
Dy2	77.97	0	77.40
Dy3	25.10	77.40	0

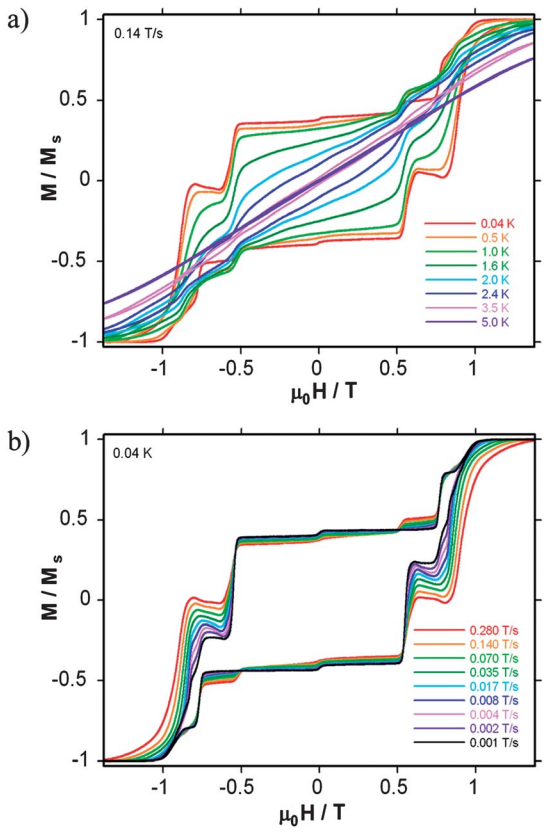

Fig. 4 Normalised magnetization (M/M_s) *vs.* applied dc field sweeps at the indicated temperatures (a) and sweep rates (b).

temperatures and increasing field sweep rates, as expected for SMM behavior. An interpretation of the hysteresis loops is given in Fig. 5. For the chosen direction of the applied magnetic field, the four **Dy_3L** molecules (denoted A–D) within a unit cell show different Zeeman spectra. Within the field interval −1.5–1.5 *T* only two of the molecules (A and B) display level crossings in the ground state, while the other two (C and D) show no intersection except at $H = 0$ (Fig. S5†). The solid line in Fig. 5 (middle plot) shows the adiabatic magnetization of one unit cell for the given direction of the applied field. The magnetic steps correspond to the level crossings in the ground state of the four **Dy_3L** molecules. For finite field sweep rates the heights of some of the magnetization steps are modified and some new steps appear due to the crossings of excited levels. The modified steps are shown in the middle plot of Fig. 5 by a green dashed line. The height of each step depends on the tunneling gap which opens at the corresponding crossing. These tunneling gaps are calculated and given in Table S5† for the chosen direction of the applied field. For instance, the first step at −1.0 *T* arises from the crossing 1A with a relatively large tunneling gap of ≈ 0.01 cm^{-1} which explains why the height of this step does not depend on the field sweep rate. The next step corresponds to the crossing 1B with a tunneling gap of 5×10^{-5} cm^{-1}, explaining why its height is strongly dependent on the field sweep rate (Fig. 4b). On the other hand, the step is very small at 0.0 *T*, because of the very small tunneling gaps in molecules A–D, which are only contributed by the environmental magnetic field.

Dy_3L is stable up to 500 K according to thermogravimetric analysis (TGA) and differential scanning calorimetry (DSC) analysis (Fig. S11†). An endothermic peak in the DSC curve was detected at *ca.* 467 K, corresponding to a first-order phase transition (Fig. S11† inset).[13] The temperature dependence of the ac dielectric constant and dielectric loss of **Dy_3L** using powder samples in pellets were measured at various frequencies from 10^2 to 10^6 Hz (Fig. 6a). With those data, the temperature-dependent ac conductivities could be calculated (Fig. S12†), in which a peak located around 470 K unambiguously appears suggesting the paraelectric–ferroelectric transition. The heights of the peaks decrease when increasing the frequencies but do not show an obvious temperature dependence. The reciprocal dielectric constant (ε') curves at 100 Hz in the temperature ranges of 446 to 460 K and 470 to 482 K are almost linear and obey the Curie–Weiss law well ($1/\varepsilon' = C/(T - T_0)$), leading to Curie constants of

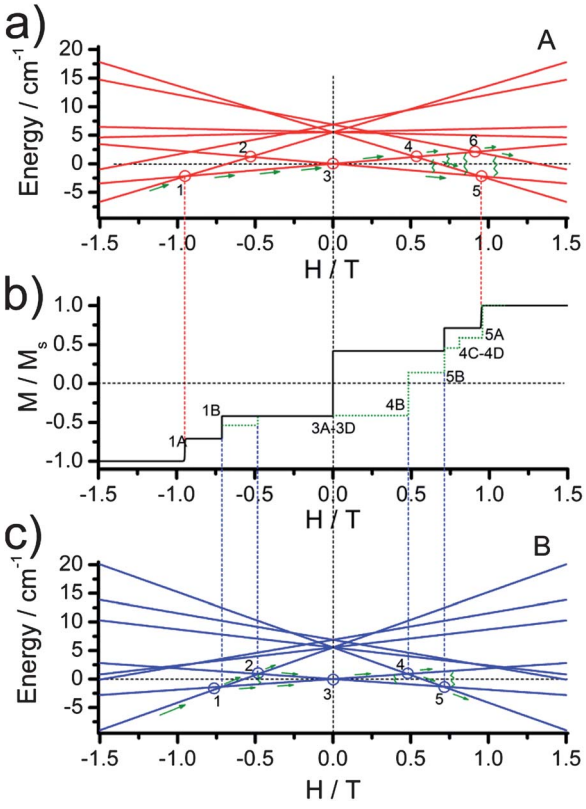

Fig. 5 a) Energy levels of the molecule **Dy_3L-A** in an applied magnetic field. (b) Molar magnetization for all four **Dy_3L** molecules (ABCD). The green dashed line shows the molar magnetization at a finite field sweep rate. (c) Energy levels of the molecule **Dy_3L-B** in an applied magnetic field. The wiggly lines show relaxation transitions from higher to lower levels.

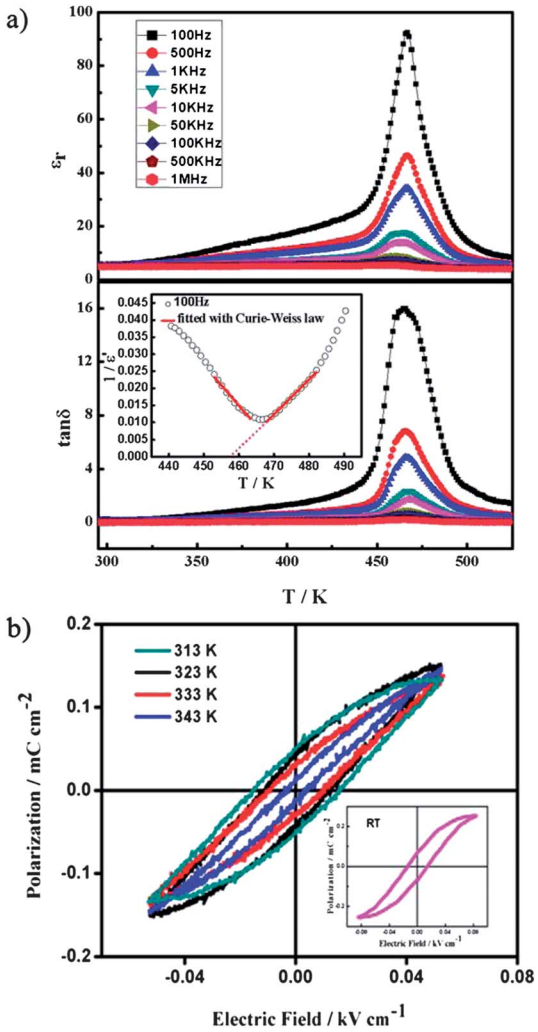

Fig. 6 a) Temperature dependence of the dielectric constant $\varepsilon'(\varepsilon_r)$ and the dielectric loss $\tan\delta$ ($\varepsilon''/\varepsilon'$) of **$Dy_3$L**. ε'' and ε' are the imaginary and real parts of the dielectric constant. Inset: the reciprocal dielectric permittivity and Curie–Weiss fit. (b) Dielectric hysteresis loops of **Dy_3L**.

$C_{ferro} = 909$ K and $C_{para} = 986$ K, and a Curie–Weiss temperature $T_0 = 457$ K (Fig. 6a, inset). The Curie constant is close to 10^3 K, which is comparable to those values for order-disorder-type molecular ferroelectrics.[13,14] The dielectric hysteresis loops of **Dy_3L** were further studied to confirm the ferroelectric nature (Fig. 6b). The hysteresis loop at room temperature shows a remnant polarization (P_r) of ~0.070 μC cm^{-2}, a coercive field (E_c) of ~0.015 kV cm^{-1}, and a saturation spontaneous polarization (P_s) of ~0.254 μC cm^{-2}. P_r and E_c values decrease with increasing temperature. The above results, as well as the extremely low leakage current (Fig. S13†) indicate the apparent ferroelectric property of **Dy_3L**. To the best of our knowledge, **Dy_3L** exhibits the highest T_c in molecular ferroelectric materials.[15] It is also noted that **Dy_3L** can be polarized by a very low applied electric field, which is energy-efficient for possible practical applications. In the solid state, the reversal of the dipoles of molecular materials results from molecular rotation/libration and/or intermolecular proton transfer.[16] For **Dy_3L** in the paraelectric phase, the disordered ethanol molecules which surround the 2_1 screw axis almost occupy the same position with contrary dipole moments. These dipole moments may be aligned to the same direction by applying an electric field to the ferroelectric phase. Hydrogen atoms of the ligand were also found to be disordered according to the crystal structural analysis, which should contribute to the dielectric hysteresis loop as well.

In conclusion, we have successfully assembled a triangular Dy(III) SMM into a polar point space group by a supramolecular approach through hydrogen bonding interactions. The interesting finding is that both SMM behaviour and ferroelectricity are observed in this single non-oxide material. To our knowledge, this is a phenomenon that has not previously been reported for a SMM also demonstrating a dielectric transition between a paraelectric and a ferroelectric phase. Although the SMM behaviour and the paraelectric–ferroelectric phase transition occur at a completely different temperature range with different origins of mechanism, this work still sheds light on a synthetic route to generate molecular multiferroic materials.

Acknowledgements

This work in China was supported by MOST (973 program, 2012CB821702), NSFC (90922032 and 21171100), 111 Project (B12015) and MOE Innovation Team (IRT0927). The work in Germany was supported by the DFG Center for Functional Nanostructures. L. U. is a post-doc of the FWO – Vlaanderen (Fonds Wetenschappelijk Onderzoek – Vlaanderen) and thanks the support from Methusalem and INPAC programs from the KU Leuven. W. W. acknowledges the ERC Advanced Grant MolNanoSpin no. 226558.

Notes and references

‡ Synthesis of **Dy_3L**: $Dy(NO_3)_3 \cdot 6H_2O$ (0.5 mmol, 228.3 mg) was slowly added to a 20 mL ethanol solution containing H_4L (1.0 mmol, 273 mg) and LiOH (0.4 mmol, 16.8 mg). The mixture was moved to a vial after two hours stirring. Colorless crystals in pure phase (checked by both carefully selection under a microscope and PXRD analysis, Fig. S14†) were obtained under 100 °C solvothermal condition three days later in a ~63% yield (based on Dy). Elemental analysis calcd (%) for **Dy_3L** ($C_{22}H_{49}Dy_3N_8O_{21}$): C, 21.15; H, 3.95; N, 8.97. Found: C, 21.68; H, 4.11; N, 8.69%. IR (KBr) for **Dy_3L**: 3447 (m), 3176 (m, br), 2950 (m, sh), 2861 (s, sh), 1511 (s), 1366 (w), 1154 (w, sh), 1089 (m, sh), 1060 (s, sh), 918 (m, sh), 817 (m, sh), 742 (m, sh), 629 ~ 458 (w, sh).

1 (*a*) I. Žutić, J. Fabian and S. Das Sarma, *Rev. Mod. Phys.*, 2004, **76**, 323–410; (*b*) L. Bogani and W. Wernsdorfer, *Nat. Mater.*, 2008, **7**, 179–186; (*c*) S. Sanvito, *Chem. Soc. Rev.*, 2011, **40**, 3336–3355.
2 (*a*) W. Eerenstein, N. D. Mathur and J. F. Scott, *Nature*, 2006, **442**, 759–765; (*b*) H. Zheng, J. Wang, S. E. Lofland, Z. Ma, L. Mohaddes-Ardabili, T. Zhao, L. Salamanca-Riba, S. R. Shinde, S. B. Ogale, F. Bai, D. Viehland, Y. Jia, D. G. Schlom, M. Wuttig, A. Roytburd and R. Ramesh, *Science*, 2004, **303**, 661–663.
3 N. A. Hill and A. Filippetti, *J. Magn. Magn. Mater.*, 2002, **242–245**, 976–979.
4 L. G. Tejuca and J. L. G. Fierro, *Perovskites and Applications of Perovskite-Type Oxides*, Marcel Dekker, New York, 1992.
5 (*a*) P. Jain, V. Ramachandran, R. J. Clark, H. D. Zhou, B. H. Toby, N. S. Dalal, H. W. Kroto and A. K. Cheetham, *J. Am. Chem. Soc.*, 2009, **131**, 13625–13627; (*b*) R. Ramesh, *Nature*, 2009, **461**, 1218–1219; (*c*) G. Rogez, N. Viart and M. Drillon, *Angew. Chem., Int. Ed.*, 2010, **49**, 1921–1923; (*d*) C.-F. Wang, Z.-G. Gu, X.-M. Lu, J.-L. Zuo and X.-Z. You, *Inorg. Chem.*, 2008, **47**, 7957–7959; (*e*) G. C. Xu, W. Zhang, X. M. Ma, Y. H. Chen, L. Zhang, H. L. Cai, Z. M. Wang, R. G. Xiong and S. Gao, *J. Am. Chem. Soc.*, 2011, **133**, 14948–14951.
6 (*a*) R. J. Blagg, C. A. Muryn, E. J. L. McInnes, F. Tuna and R. E. P. Winpenny, *Angew. Chem., Int. Ed.*, 2011, **50**, 6530–6533; (*b*) I. J. Hewitt, Y. H. Lan, C. E. Anson, J. Luzon, R. Sessoli and A. K. Powell, *Chem. Commun.*, 2009, 6765–6767; (*c*) I. J. Hewitt, J. K. Tang, N. T. Madhu, C. E. Anson, Y. H. Lan, J. Luzon, M. Etienne, R. Sessoli and A. K. Powell, *Angew. Chem., Int. Ed.*, 2010, **49**, 6352–6356.
7 C. Benelli and D. Gatteschi, *Chem. Rev.*, 2002, **102**, 2369–2387.
8 J. K. Tang, I. Hewitt, N. T. Madhu, G. Chastanet, W. Wernsdorfer, C. E. Anson, C. Benelli, R. Sessoli and A. K. Powell, *Angew. Chem., Int. Ed.*, 2006, **45**, 1729–1733.
9 (*a*) L. F. Chibotaru, L. Ungur and A. Soncini, *Angew. Chem., Int. Ed.*, 2008, **47**, 4126–4129; (*b*) J. Luzon, K. Bernot, I. J. Hewitt, C. E. Anson, A. K. Powell and R. Sessoli, *Phys. Rev. Lett.*, 2008, **100**, 247205–247208.
10 (*a*) P. H. Lin, T. J. Burchell, L. Ungur, L. F. Chibotaru, W. Wernsdorfer and M. Murugesu, *Angew. Chem., Int. Ed.*, 2009, **48**, 9489–9492; (*b*) Y. N. Guo, G. F. Xu, P. Gamez, L. Zhao, S. Y. Lin, R. Deng, J. K. Tang and H. Zhang, *J. Am. Chem. Soc.*, 2010, **132**, 8538–8539.
11 M. Hagiwara, *J. Magn. Magn. Mater.*, 1998, **177–181**, 89–90.
12 W. Wernsdorfer, *Adv. Chem. Phys.*, 2001, **118**, 99–190.
13 W. Zhang and R.-G. Xiong, *Chem. Rev.*, 2012, **112**, 1163–1195.
14 S. O. Kasap and P. Capper, *Springer Handbook of Electronic and Photonic Materials*, Springer, New York, 2006.
15 T. Hang, W. Zhang, H. Y. Ye and R. G. Xiong, *Chem. Soc. Rev.*, 2011, **40**, 3577–3598.
16 S. Horiuchi, Y. Tokunaga, G. Giovannetti, S. Picozzi, H. Itoh, R. Shimano, R. Kumai and Y. Tokura, *Nature*, 2010, **463**, 789–792.

